Electronic Supplementary Material (ESI) for Nanoscale.
This journal is © The Royal Society of Chemistry 20xx

Supporting Information

Cerium vanadate/S heterostructure for long-life zinc-ion battery: efficient electron transfer by the anchored sulfur

Yuan Li, Kai Li, Yang Liu and Yun Gong*

Department of Applied Chemistry, College of Chemistry and Chemical Engineering, Chongqing University, Chongqing 401331, P. R. China Tel: +86-023-65678932 E-mail: gongyun7211@cqu.edu.cn

Experimental methods

Materials

Vanadium pentoxide (V_2O_5) and hydrogen peroxide (H_2O_2, 30%) were purchased from Chengdu Cologne Chemicals Co., Ltd. Cerium(IV) sulfate tetrahydrate ($Ce(SO_4)_2{\cdot}4H_2O$) was obtained from Aladdin Co., Ltd. All the reagents used in the experiment were analytical grade and directly used without further purification. Zn foil (thickness: 0.1 mm) was purchased from Runde Metal Materials Co., Ltd. Carbon cloth (W0S1009, thickness: 0.1 mm) was obtained from Suzhou Sinero Technology Co., Ltd. Glass fiber membrane (Grade GF/C) was purchased from Whatman Company.

Synthesis of VS_2

VS_2 was synthesized according to the literature with a little modification.[1-3] In a typical procedure, 6 mmol NH_4VO_3 and 32 mmol thioacetamide (TAA) were dispersed in the mixed solvent which was composed of 45 mL water and 9 mL $NH_3{\cdot}H_2O$ under stirring, then the mixture was transferred to a 50 mL Teflon-lined steel autoclave and kept at 160 ℃ for 20 h. After natural cooling to room temperature, the obtained precipitate was separated by centrifugation, then thoroughly washed with distilled water, followed by a small amount of ethanol, and dried in vacuum at 60 ℃ for 5 h.

Syntheses of $Ce_{0.25}V_2O_5(H_2O){\cdot}H_2O$ (CeVO) and $Ce_{0.3}V_2O_5(H_2O){\cdot}H_2O$/S (CeVS)

CeVO and CeVS were synthesized through a conventional hydrothermal method. In a typical synthesis, 50 mg of V_2O_5, 9.5 mL deionized water, and 0.5 mL H_2O_2 (30

%) were dispersed in a beaker under ultrasonication for 20 min to form a homogeneous solution. Then, 50 mg of $Ce(SO_4)_2 \cdot 4H_2O$ powder was added to the solution under sonication for another 20 minutes. Afterward, the obtained transparent solution was transferred into a 10 mL Teflon-lined autoclave and heated at 150 ℃ for 12 h. After natural cooling, the obtained precipitate was washed by distilled water and ethanol three times separately, then frozen and underwent a freeze-drying process.

The synthesis of CeVS was similar to that of CeVO except that VS_2 (50 mg) was utilized instead of V_2O_5 (50 mg), and the obtained sample was successively washed by distilled water, CS_2 and ethanol before freeze-drying process.

Synthesis of $V_2O_5 \cdot nH_2O$

The synthesis of $V_2O_5 \cdot nH_2O$ was similar to that of CeVO but in the absence of $Ce(SO_4)_2 \cdot 4H_2O$.

Material Characterizations

The structure properties were identified on powder X-ray diffractometer (XRD) (PANalytical X'pert Pro MPD) with Cu Kα radiation (λ = 1.54056 Å) at 40 kV and 30 mA. The metallic elemental compositions of the samples were measured on inductively coupled plasma optical emission spectroscopy (ICP-OES 6300 Duo, Thermo). Raman spectra were conducted on a Renishaw Raman spectrometer with the wavenumber ranging from 100 to 1200 cm^{-1}. X-ray photoelectron spectroscopy (XPS) was carried out on a ESCALAB 250 analyzer. The content of S was measured on a Unicube Elemental Analyzer (Elementar Analysensysteme GmbH, Germany). Thermogravimetric (TG) curves were measured on a METTLER TOLEDO TGA2 analyzer. Electron paramagnetic resonance (EPR) were measured on EPR200-Plus with the sweep width of 100 G. The scanning electron microscopy (SEM, with an accelerating voltage of 20 kV) and energy-dispersive X-ray (EDS) analyses and elemental mapping images of the samples were obtained from Thermo Fisher (Quattro S) instrument equipped with an EDS (AMETEK) analyzer. Transmission electron microscopy (TEM), high resolution TEM (HRTEM) as well as selected area electron diffraction (SAED) patterns were ascertained by a Thermo Fisher Talos F200s apparatus equipped with an EDS analyzer (Super-X).

Electrochemical Measurements

The cathode was prepared as follows: The active material, graphite powder, acetylene black (AB), and polyvinylidene fluoride (PVDF) with a weight ratio of 5: 2: 2: 1 were thoroughly mixed in N-methyl-2-pyrrolidone (NMP) solvent. Afterward, the

obtained slurry was dropped on a carbon cloth (CC) (12 mm in diameter) and dried at 75 °C for 12 h in a vacuum oven. The mass loading of active material is around 1.2 ~ 2.0 mg cm^{-2}. The electrochemical measurements were carried out in coin-type cells (CR2032), which were assembled in air, using Zn foil as anode, glass fiber filter as separator, and 3 M $Zn(CF_3SO_3)_2$ aqueous solution as electrolyte.

The redox property was measured by cyclic voltammetry (CV) on a CHI660E electrochemical workstation. Electrochemical impedance spectroscopy (EIS) were conducted between 100 kHz to 0.01 Hz on the CHI660E electrochemical workstation as well. The galvanostatic charge/discharge (GCD) tests and galvanostatic intermittent titration technique (GITT) measurements were performed using CT2001A LAND instrument, and the voltage was set from 0.2 and 1.6 V vs Zn^{2+}/Zn. The rate performances were tested between 0.1 to 5.0 A g^{-1}. The GITT measurement was performed at 0.1 A g^{-1} during the 2^{nd} cycle. The cell was galvanostatic discharged/charged at 0.1 A g^{-1} for 10 min, and then relaxed for 10 min and followed by a relaxation to reach equilibrium. This process was repeatedly applied until the charge/discharge voltage reached 1.6/0.2 V.

Density functional theory (DFT) calculations

The calculation program was performed according to the Vienna ab initio simulation package (VASP).[4-7] The electronic exchange correlation energy is treated in the scheme of the Perdew-Bruke Ernzerhof (PBE) version of Generalized Gradient Approximation (GGA). The cutoff energy of plane-wave function was set to be 400 eV. The total energy and the residual force on the atom were converged below 10^{-5} eV per atom and smaller than 0.02 eV $Å^{-1}$, respectively. 3 × 3 × 3 Monkhorst−Pack k-point grids were applied to sample for Brillouin-zone integration.

The binding energy (ΔE) for the intercalation of Zn^{2+} into the inner channel of $Ce_{0.25}V_2O_5(H_2O)\cdot H_2O$ (CeVO) was calculated as following:

$$\Delta E = [E(\text{CeVO} / x\ \text{Zn}) - E(\text{CeVO}) - x\ E(\text{Zn})] / x$$

Where E(CeVO / x Zn) is the total energy after Zn^{2+} intercalated into CeVO,

whereas *E*(CeVO) is the energy of the individual CeVO. And *E* (Zn) is the energy per Zn atom (hcp).

The diffusion energy (E) was calculated according to the follow equation:

$E = E_{max} - E_{ini}$

Where E_{max} and E_{ini} are the maximal energy (transition state, TS) and the initial state (IS) energy during the zinc-ion diffusion, respectively. The initial state (IS) can be considered as the state that Zn^{2+} ion hasn't been intercalated into the sample.

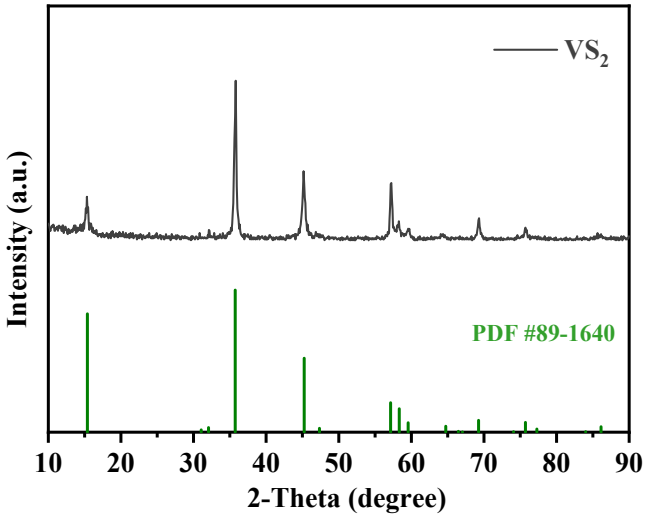

Fig. S1 XRD patterns of the prepared VS_2 and the standard profile (PDF #89-1640).

Table S1 The contents of Ce and V in CeVS and CeVO.

Sample	Element	μg ml^{-1}	μmol ml^{-1}
CeVO	Ce	4.622	0.033
	V	17.94	0.352
CeVS	Ce	5.508	0.039
	V	18.23	0.358

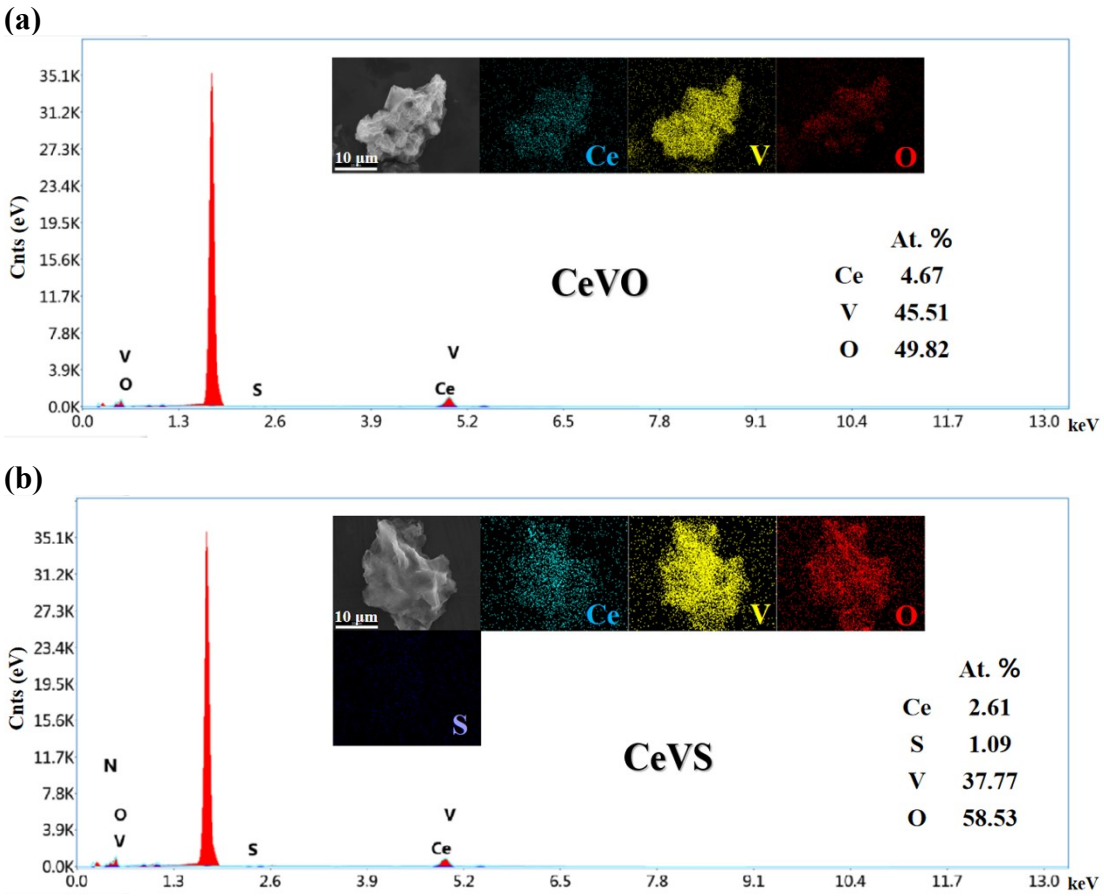

Fig. S2 EDS and elemental mappings of (**a**) CeVO and (**b**) CeVS.

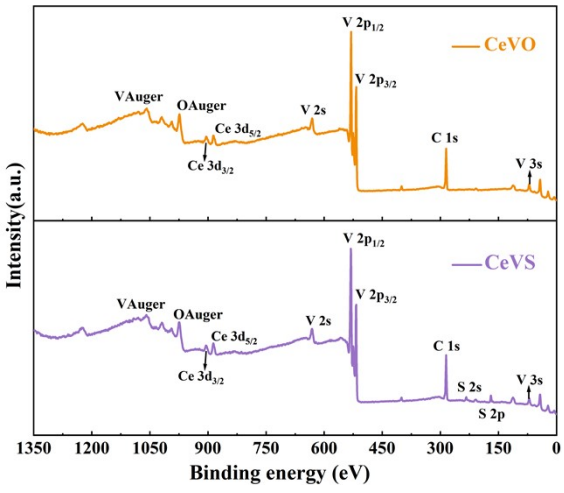

Fig. S3 XPS survey spectra of CeVS and CeVO.

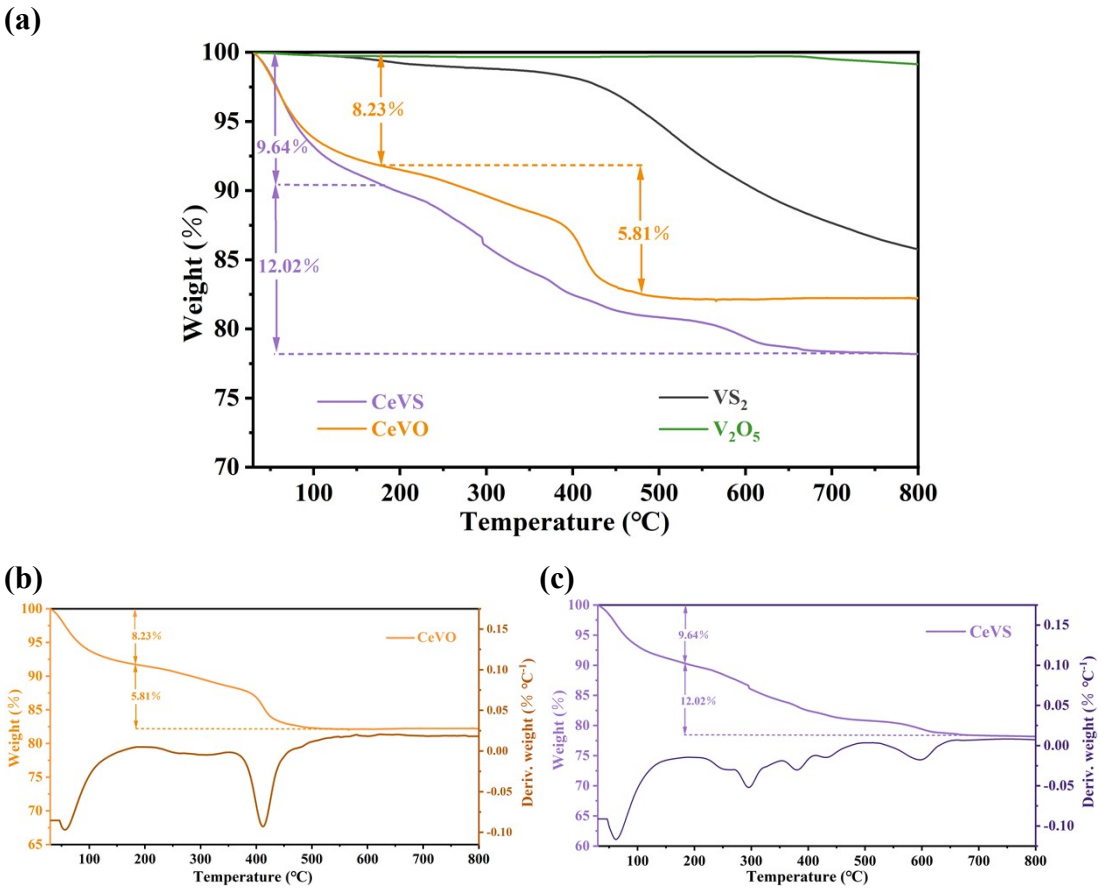

Fig. S4 (**a**) TG curves of CeVO, CeVS, V_2O_5 and VS_2. TG as well as DTG curves of (**b**) CeVO and (**c**) CeVS.

S1 Synthesis and characterization of $V_2O_5 \cdot nH_2O$

Synthesis of $V_2O_5 \cdot nH_2O$

The synthesis of $V_2O_5 \cdot nH_2O$ was similar to that of CeVO but in the absence of $Ce(SO_4)_2 \cdot 4H_2O$.

The characterization of $V_2O_5 \cdot nH_2O$

The XRD patterns of the commercial V_2O_5 and the as-prepared $V_2O_5 \cdot nH_2O$ are shown in **Fig. S5**. It can be seen that the commercial V_2O_5 is attributed to the orthorhombic V_2O_5 (JCPDS No. 72-0433). However, the XRD pattern the as-prepared $V_2O_5 \cdot nH_2O$ exhibits a different XRD pattern, in which a diffraction peak is observed at 7.6 °, suggesting that it possesses a largest interlayer spacing of 11.7 Å due to the pre-intercalation of water.

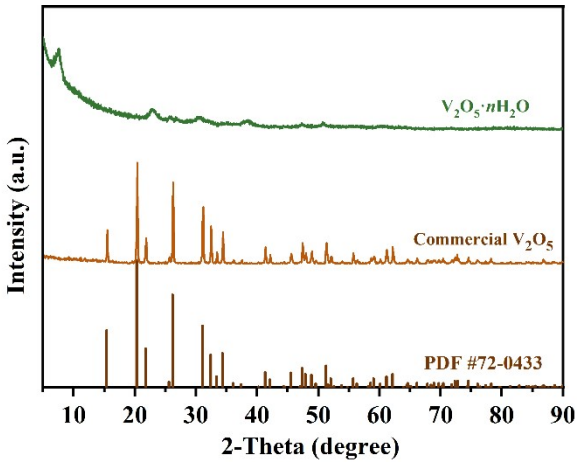

Fig. S5 XRD patterns of $V_2O_5 \cdot nH_2O$, the commercial V_2O_5 and the standard profile (JCPDS No. 72-0433).

Table S2 Comparison of the vanadium-based cathodes in aqueous ZIBs.

Material	**Specific capacity (mAh g^{-1})**	**Cycle number**	**Capacity retention**	**Reference**
VS_2/VO_x	260@ 0.1 A g^{-1}	3000 (1 A g^{-1})	75.0 %	3
$Zn_{0.25}V_2O_5 \cdot nH_2O$	282@ 0.3 A g^{-1}	1000 (2.4 A g^{-1})	80.0 %	8
VOH-PPy	422@ 0.1 A g^{-1}	5000 (10.0 A g^{-1})	53.9 %	9
VS_2 nanospheres	212.9@ 0.1 A g^{-1}	2000 (2 A g^{-1})	86.7 %	10
$Co_{0.24}V_2O_5 \cdot 0.944H_2O$	432@ 0.1 A g^{-1}	7500 (10 A g^{-1})	90.3 %	11
PVO	258@ 0.1 A g^{-1}	100 (0.1 A g^{-1})	91.5%	12
$H_{11}Al_2V_6O_{23.2}$	288.4@ 0.1 A g^{-1}	7000 (5 A g^{-1})	88.6 %	13
$Mg_{0.23}V_2O_5 \cdot 1.0H_2O$	393@ 0.2 A g^{-1}	2000 (5.0 A g^{-1})	98.6 %	14
GP-HVO_d	402.5@ 0.2 A g^{-1}	200 (0.2A g^{-1})	99.7 %	15
KNVO	464@ 0.1 A g^{-1}	3000 (5.0 A g^{-1})	90.0 %	16
VO-PBAs	209.6 @ 0.1 A g^{-1}	2000 (1.0 A g^{-1})	95.5 %	17
CeVS	**438@ 0.1 A g^{-1}**	**10500 (5 A g^{-1})**	**100.0 %**	**Our work**

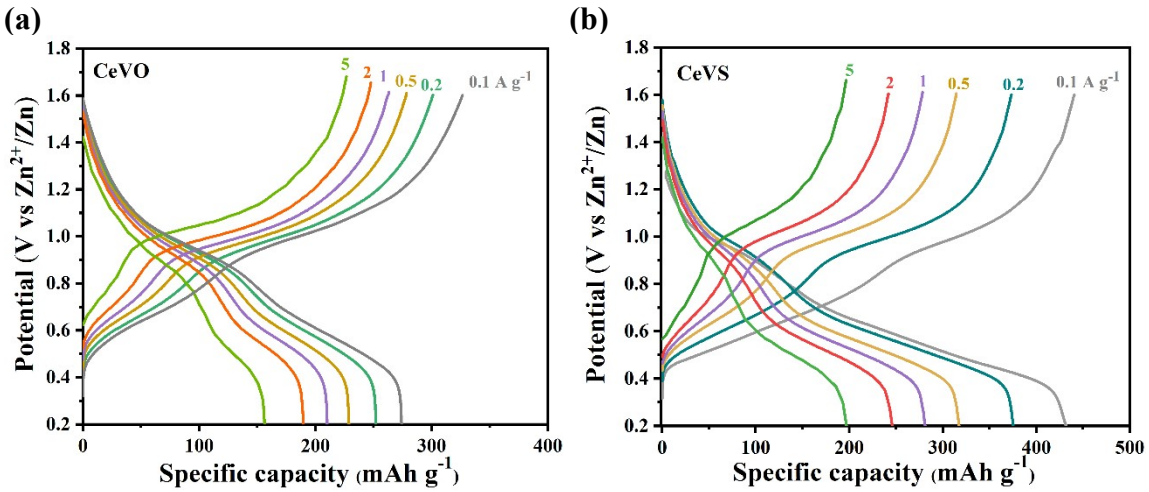

Fig. S6 GCD curves of (**a**) CeVO and (**b**) CeVS at the current densities from 0.1 to 5 A g^{-1}.

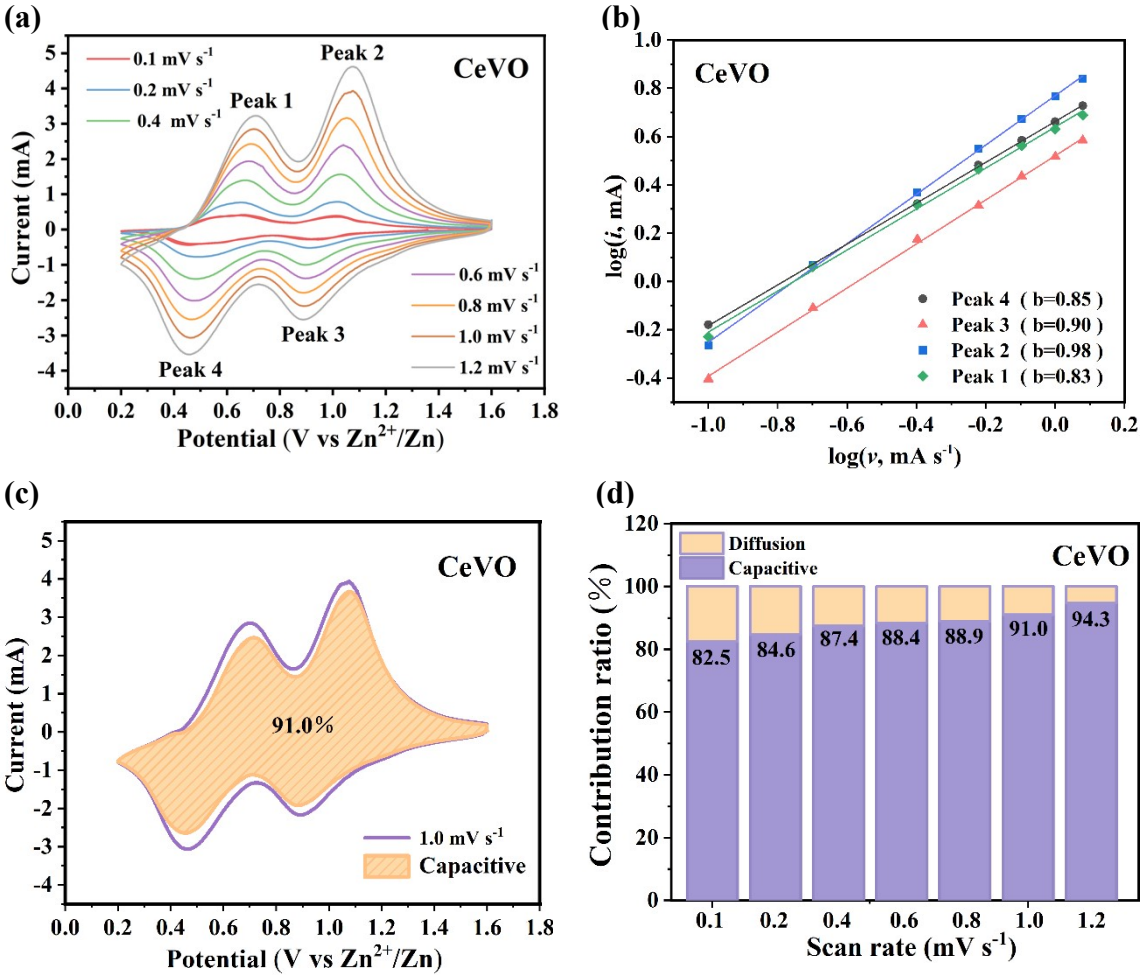

Fig. S7 Electrochemical performance of CeVO: (**a**) CV curves at various scan rates; (**b**) Log (*i*) vs log (*v*) plots of the four redox peaks in **a**; (**c**) The contribution ratios of the pseudocapacity at 1.0 mV s^{-1} and (**d**) different scan rates.

Table S3 The parameters in the equivalent circuit of CeVS and CeVO.

Sample	R_s (Ω cm^{-2})	R_{ct} (Ω cm^{-2})	CPE	W (Ω cm^{-2})
CeVS	1.97	7.98	1.11×10^{-3}	14.90
CeVO	2.16	18.35	1.71×10^{-2}	70

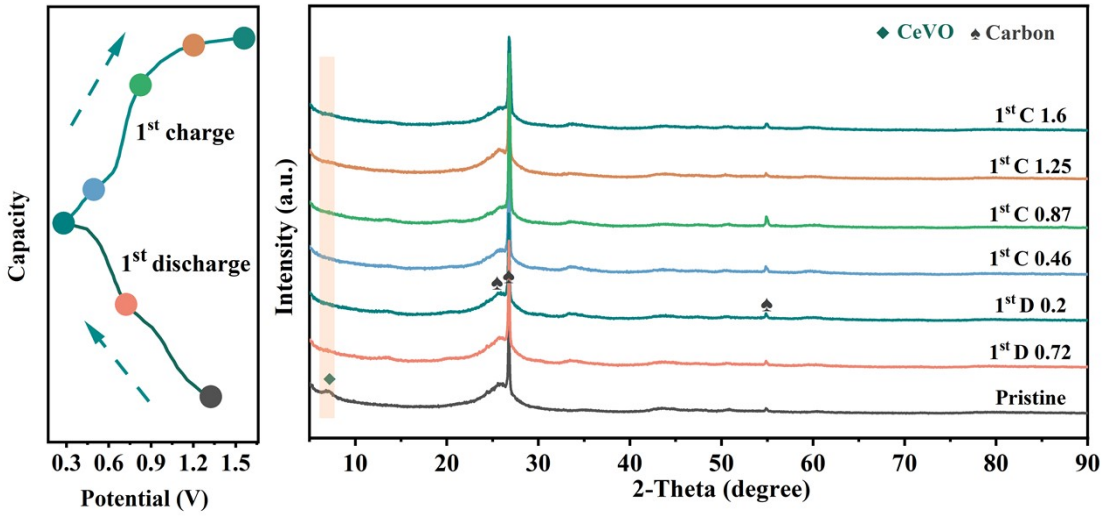

Fig. S8 *Ex-situ* XRD patterns of CeVO at 0.1 A g^{-1} during 1st discharge/charge cycle.

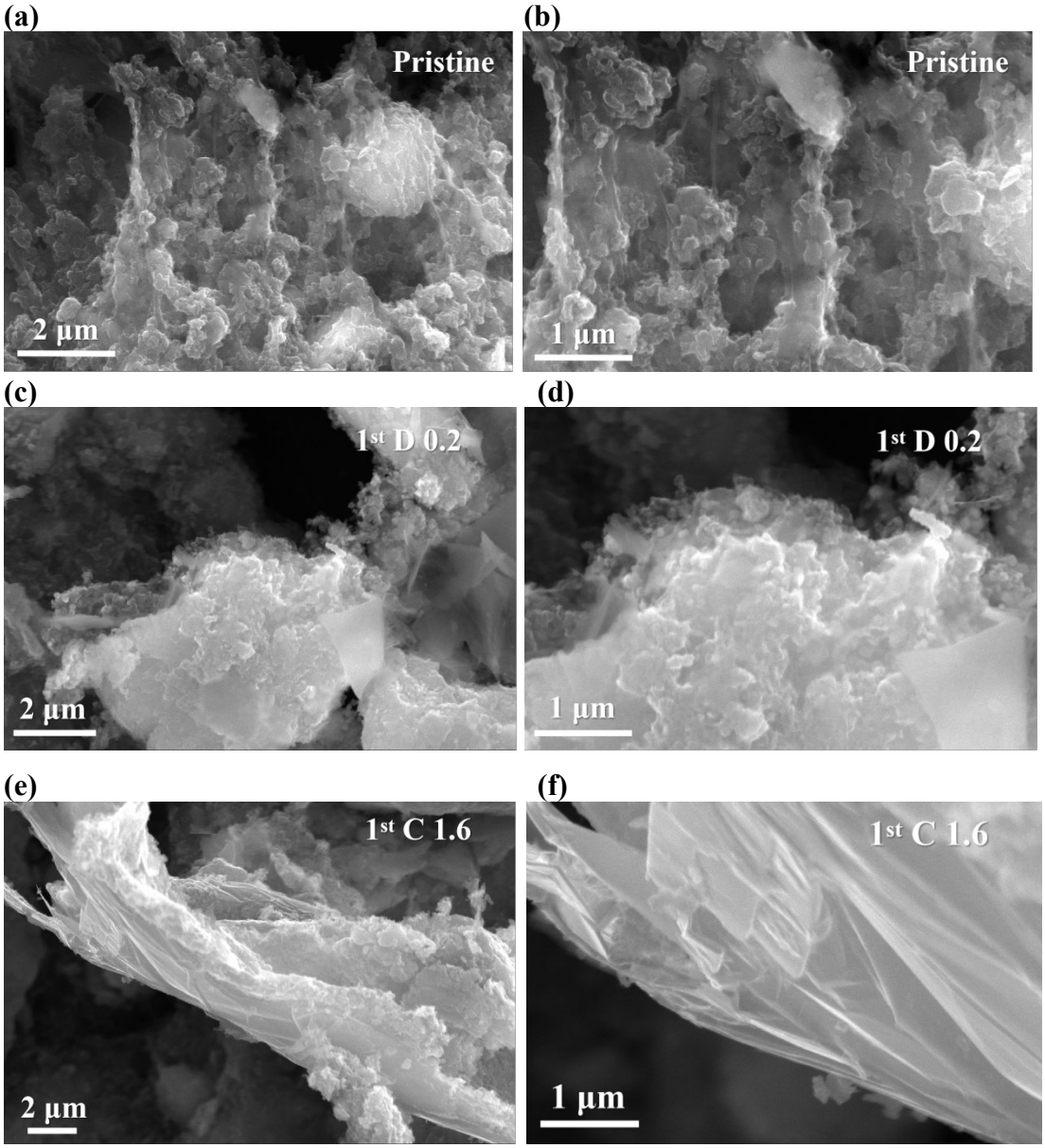

Fig. S9 SEM images of the CeVS electrode at different states: (**a, b**) the pristine electrode; (**c, d**) the 1st discharged to 0.2 V and (**e, f**) charged to 1.6 V.

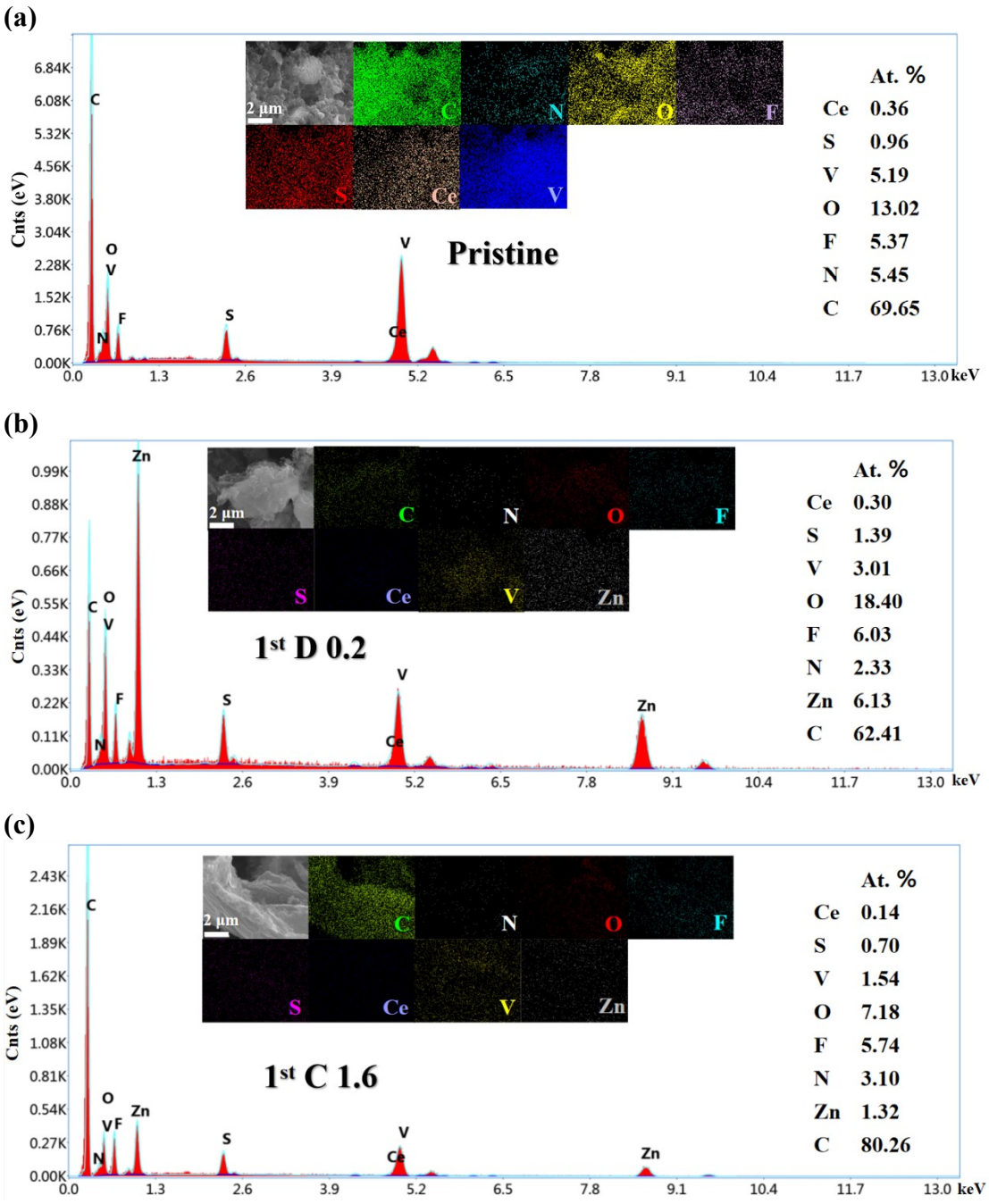

Fig. S10 EDS and elemental mappings of the CeVS electrode at different states: (**a**) the pristine electrode; (**b**) the 1st discharged to 0.2 V and (**c**) charged to 1.6 V.

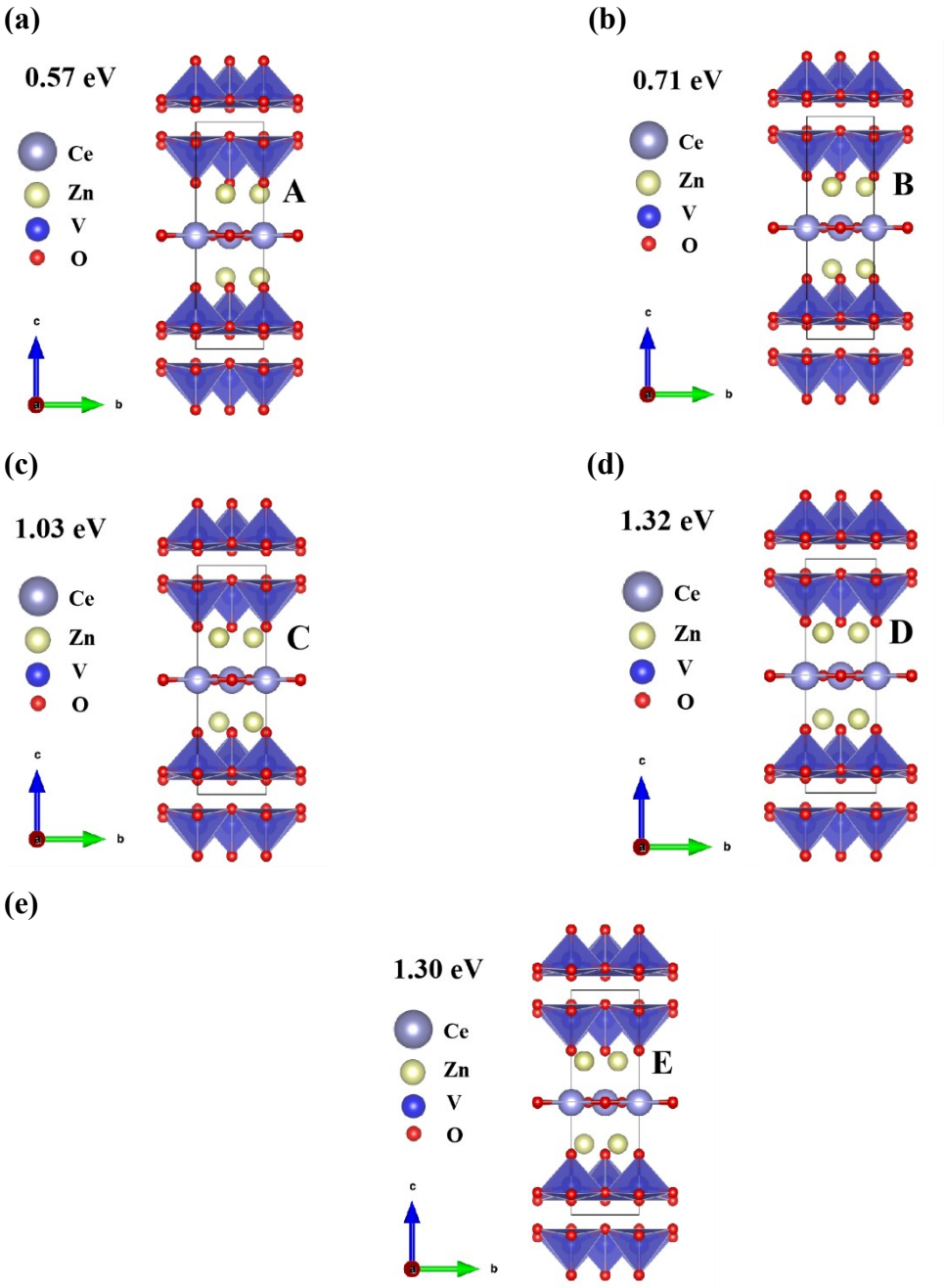

Fig. S11 The optimized configurations with Zn^{2+} across sites (**a**) A, (**b**) B, (**c**) C, (**d**) D and (**e**) E in the CeVO cell.

References

1. X. Zhang, Q. He, X. M. Xu, T. F. Xiong, Z. T. Xiao, J. S. Meng, X. P. Wang, L. Wu, J. H. Chen and L. Q. Mai, *Advanced Energy Materials*, 2020, **10**, 1904118.
2. D. X. Yu, Q. Pang, Y. Gao, Y. J. Wei, C. Z. Wang, G. Chen and F. Du, *Energy Storage Materials*, 2018, **11**, 1-7.

3. D. X. Yu, Z. X. Wei, X. Y. Zhang, Y. Zeng, C. Z. Wang, G. Chen, Z. X. Shen and F. Du, *Advanced Functional Materials*, 2021, **31**, 2008743.
4. L. F. Hu, Z. Y. Wu, C. J. Lu, F. Ye, Q. Liu and Z. M. Sun, *Energy & Environmental Science*, 2021, **14**, 4095-4106.
5. R. Wang, H. C. Yang, N. D. Lu, S. L. Lei, D. L. Jia, Z. X. Wang, Z. H. Liu, X. G. Wu, H. Z. Zheng, S. Ali, F. Ma and S. L. Peng, *Chemical Engineering Journal*, 2022, **433**, 134500.
6. Z. P. Jiang, Z. Q. Zeng, X. M. Liang, L. Yang, W. Hu, C. Zhang, Z. L. Han, J. W. Feng and J. Xie, *Advanced Functional Materials*, 2021, **31**, 2005991.
7. J. An, L. Y. Shi, G. R. Chen, M. S. Li, H. J. Liu, S. Yuan, S. M. Chen and D. S. Zhang, *Journal of Materials Chemistry A*, 2017, **5**, 19738-19744.
8. D. Kundu, B. D. Adams, V. Duffort, S. H. Vajargah and L. F. Nazar, *Nature Energy*, 2016, **1**, 16119.
9. Z. Y. Feng, J. J. Sun, Y. Y. Liu, H. M. Jiang, M. Cui, T. Hu, C. G. Meng and Y. F. Zhang, *Acs Applied Materials & Interfaces*, 2021, **13**, 61154-61165.
10. Y. Tan, S. W. Li, X. D. Zhao, Y. Wang, Q. Y. Shen, X. H. Qu, Y. C. Liu and L. F. Jiao, *Advanced Energy Materials*, 2022, **31**, 2104001.
11. L. T. Ma, N. Li, C. B. Long, B. B. Dong, D. L. Fang, Z. X. Liu, Y. W. Zhao, X. L. Li, J. Fan, S. M. Chen, S. J. Zhang and C. Y. Zhi, *Advanced Functional Materials*, 2019, **29**, 1906142.
12. Z. Q. Wang, X. Y. Tang, S. Yuan, M. Bai, H. L. Wang, S. Y. Liu, M. Zhang and Y. Ma, *Advanced Functional Materials*, 2021, **31**, 2100164.
13. T. Y. Wei, Y. Y. Liu, G. Z. Yang and C. X. Wang, *Energy Storage Materials*, 2020, **30**, 130-137.
14. W. W. Xu, C. Z. Liu, Q. L. Wu, W. W. Xie, W. Y. Kim, S. Y. Lee and J. Gwon, *Journal of Materials Chemistry A*, 2020, **8**, 18327-18337.
15. J. T. Huang, H. P. Liang, Y. Tang, B. A. Lu, J. Zhou and S. Q. Liang, *Advanced Energy Materials*, 2022, **31**, 2201434.
16. Q. Zong, Q. Q. Wang, C. F. Liu, D. W. Tao, J. Y. Wang, J. J. Zhang, H. W. Du, J. F. Chen, Q. L. Zhang and G. Z. Cao, *Acs Nano*, 2022, **16**, 4588-4598.
17. Y. P. Tian, M. M. Ju, X. Q. Bin, Y. J. Luo and W. X. Que, *Chemical Engineering Journal*, 2022, **430**, 132864.